

Soft-Switched Square-Wave Half-Bridge DC-DC Converter

CHARLES R. SULLIVAN, Member, IEEE

SETH R. SANDERS, Member, IEEE
University of California

A constant-frequency zero-voltage-switched square-wave dc-dc converter is introduced, and results from experimental half-bridge implementations are presented. A nonlinear magnetic element produces the advantageous square waveforms, and provides isolated terminals from which the output voltage may be controlled. Semiconductor stresses and losses are minimized both by the square waveforms and by low switching losses. The active switches and the output rectifiers both exhibit zero-voltage switching. The active switches (metal-oxide-semiconductor field-effect transistors (MOSFETs)) are operated at a fixed frequency with 50% duty cycle, which allows the use of a simple open-loop gate drive. Experimental implementations verify predicted operation.

Manuscript received August 9, 1994; revised February 23, 1996.

IEEE Log No. T-AES/33/2/1/03152.

The work of C. R. Sullivan was supported by an NSF Graduate Fellowship.

Authors' addresses: C. R. Sullivan, Thayer School of Engineering, 8000 Cummings Hall, Dartmouth College, Hanover, NH 03755; S. R. Sanders, Dept. of Electrical Engineering and Computer Sciences, 211-73 Cory Hall #1772, University of California, Berkeley, Berkeley, CA 94720.

0018-9251/97/\$10.00 © 1997 IEEE

I. INTRODUCTION

This paper introduces a constant-frequency zero-voltage-switched square-wave dc-dc converter and presents results from experimental half-bridge implementations. The circuit is built with a saturating magnetic element that provides a mechanism to effect both soft switching and control. The square current and voltage waveforms result in low voltage and current stresses on the primary switch devices and on the secondary rectifier diodes, equal to those in a standard half-bridge pulsewidth modulated (PWM) converter. The primary active switches exhibit zero-voltage switching. The output rectifiers also exhibit zero-voltage switching. (In a center-tapped secondary configuration the rectifier does have small switching losses due to the finite leakage inductance between the two secondary windings on the transformer.) The VA rating, and hence physical size, of the nonlinear reactor is small, a fraction of that of the transformer in an isolated circuit. The active switches (metal-oxide-semiconductor field-effect transistors (MOSFETs)) are operated open loop at a fixed frequency with 50% duty cycle. Control can be effected by varying the dc current in an auxiliary winding on the nonlinear reactor.

A plethora of soft-switched and/or resonant converter circuits have emerged over the last ten years. To the best of the authors' knowledge, there is no constant-frequency soft-switched half-bridge circuit featuring square current waveforms and simple control. The circuit introduced here is expected to be of use where power levels cannot justify use of a full bridge configuration. In addition, the control and gate drive scheme is considerably simpler than that typically used in soft-switched full-bridge converters. A number of authors [1-4] have reported on soft-switched full-bridge circuits that rely on phase-shifting between the legs of the bridge for control. A potential difficulty with this class of circuits is the complexity of the gate drive timing. In particular, in these designs, commutation is achieved via the ringing of leakage inductance (or an auxiliary commutating inductor) and switch capacitance. Careful timing needs to be implemented to allow for zero-voltage transitions. These circuits typically exhibit rectifier switching losses. In any case, phase-shifting is not possible with a half-bridge configuration.

One class of circuits that has emerged in the literature [5-7] is similar to the circuit introduced here. The class of circuits in [5-7] features square waveforms and zero-voltage switching for the primary switch devices. This is accomplished through the use of nonlinear reactors. The nonlinear reactors are configured differently, but serve similar functions to those in the circuit introduced here. However, in the simple form of the circuits in [5-7], the secondary rectifier devices exhibit lossy turn-off transitions.

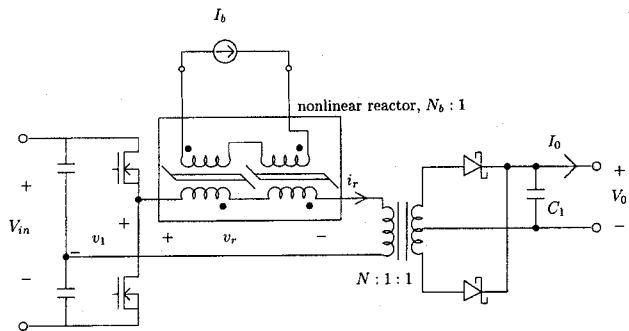


Fig. 1. Soft-switched square-wave half-bridge dc-dc converter.

The circuit introduced here is also similar to multiple-output PWM circuits that use mag-amp post-regulators for some of the outputs. The circuit could be considered an altered version of a half-bridge mag-amp circuit. Half-bridge mag-amp circuits have many disadvantages, as discussed in detail in [8]. Many of these problems result from the use of PWM in the primary circuit. Because the circuit introduced here uses a constant 50% duty cycle, it avoids problems with undesired circulating currents during the off time of the PWM. There is no requirement for a freewheeling diode on the output, and in fact the absence of a freewheeling diode is beneficial in forcing full load current to effect zero-voltage switching.

Another similar use of a saturating reactor is suggested in the recent paper of Cuk, et al. [9]. This work relies on controlling the reluctance of an auxiliary leg of a transformer core to control the leakage between primary and secondary windings wound on separate legs of this core. The reluctance of the auxiliary leg, and hence the leakage inductance, is controlled by a dc bias winding used to saturate this auxiliary leg.

There have also been a large number of publications on soft-switched single-ended circuits. The single-ended circuits that most closely resemble the work reported here are in [10, 11]. The paper of Erickson, et al. [10] used a nonlinear reactor to clamp a resonant current waveform in a zero-current-switched

single-ended circuit. This function of a nonlinear reactor is similar to that of the nonlinear reactor in the present work.

II. CIRCUIT DESCRIPTION

The circuit of Fig. 1 is built from three stages, as are most resonant dc-dc converters. The front end is a half-bridge inverter, while the output stage is a capacitor-loaded center tapped half-bridge rectifier. The salient element of the schematic in Fig. 1 is the nonlinear reactor, shown enclosed in a box. With constant secondary bias current of I_b , the flux-current characteristic at the primary terminals of this reactor has the form shown in Fig. 2(c). This characteristic is the result of combining the flux-current characteristics of the two cores, Fig. 2(a) and (b) (each shifted appropriately to account for the effect of the bias windings), by summing the two flux values at each current point. For this circuit, it is desirable to operate the reactor with the flux within the bounds of the indicated maximum operating range. The reactor has its incremental inductance increase greatly when a current threshold ($I_b N_b$) is reached. This clamps the current in the primary winding of the reactor near this current level ($I_b N_b$), and thus gives the converter its advantageous square current waveforms.

The action of the nonlinear reactor can be viewed as follows. If the reactor is driven with a 50% duty cycle square-wave voltage with zero dc component, one would expect to observe a similar square current waveform that is delayed by a quarter cycle with respect to the drive waveform. The magnitude of the current waveform is determined entirely by the secondary bias current. When inserted in the half-bridge circuit of Fig. 1, the nonlinear reactor faces the sum of the square primary voltage waveform and a square voltage waveform reflected from the secondary. The reflected secondary voltage waveform is approximately in phase with the reactor current since the capacitor-loaded rectifier is current-controlled from the nonlinear reactor. Hence, ideal waveforms for the

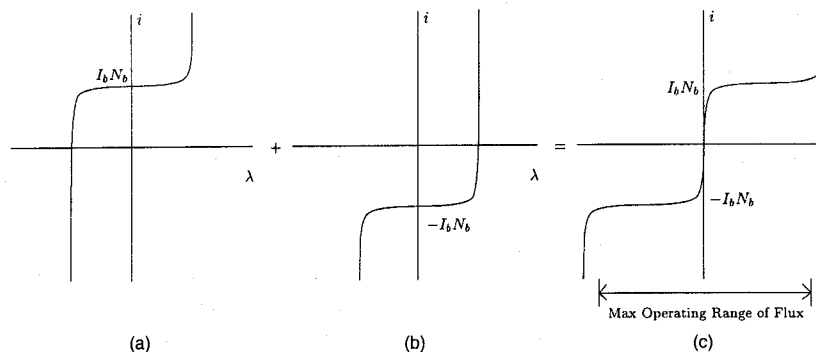


Fig. 2. Flux-current characteristic of saturating reactor. (a) and (b) are characteristics of individual cores, which are added together to find characteristic of composite reactor, (c).

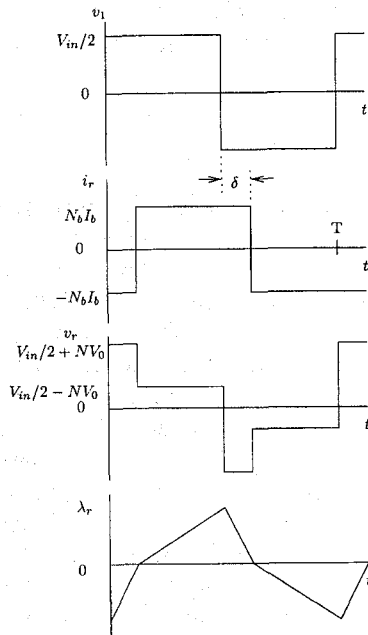


Fig. 3. Ideal circuit waveforms.

reactor are as shown in Fig. 3. As such, the reactor current always lags the voltage square wave applied by the active half-bridge, and zero-voltage switching is readily effected.

The control of the output voltage or current is effected by controlling the current in a secondary winding on the nonlinear reactor, and hence, there is no need for any additional control mechanism in the active bridge circuit. The gate drive may operate open-loop, with constant duty cycle. Ideally, the reactor clamps the the primary current to plus or minus $N_b I_b$. The rectifier and transformer convert this into a constant positive current of $N_b N I_b$. In practice the output current is somewhat less than this because of the the current needed to charge and discharge the capacitance of the output rectifiers during commutation of the reactor current, the magnetizing current of the transformer, and the deviations of the nonlinear reactor characteristic from an ideal, square, single-valued $\lambda - i$ characteristic. As discussed above, the nonlinear reactor serves to introduce a delay between the driving voltage square wave and the reactor current, and hence the transformer primary voltage square wave. From considering the reactor flux, it can be shown that the delay, δ , must satisfy the constraint,

$$(V_{in}/2 + NV_0)\delta = (V_{in}/2 - NV_0)(T/2 - \delta). \quad (1)$$

When the output voltage is adjusted via the bias current, δ adjusts accordingly. Hence, voltage regulation is accompanied by phase shift between inverter voltage and primary current. In particular, for maximum output voltage, the phase shift is near zero, and for zero output voltage, the phase shift is 90 deg.

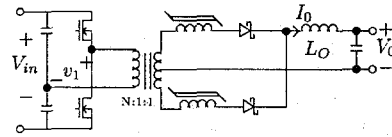


Fig. 4. A similar circuit.

Since the secondary rectifier is current fed and capacitor loaded, it also exhibits zero-voltage transitions, as long as the two secondary windings are tightly coupled. This is not unlike the rectifier switching behavior in a capacitor-loaded series resonant converter. The rectifier load capacitor may be small because it only handles short-duration transient currents that are generated during the commutation of the nonlinear reactor and rectifier combination.

The ratings of the major components are very similar to those of a PWM forward converter. Suppose the circuit is run with an output voltage of V_O , an output current of I_O , and a conversion ratio of $\gamma/(2N)$, i.e., $V_O = V_{in}\gamma/(2N)$. Here, N is the transformer turns ratio, γ accounts for regulation accomplished with the nonlinear reactor, and the factor of two accounts for the half-bridge configuration. The primary switches experience a peak voltage-current stress product of $2V_O/\gamma \cdot I_O$. The main transformer primary sees a peak flux-current stress of $(V_O T/4) \cdot I_O$. A practical current source for the bias winding will incorporate an inductor. This component may be compared to the output choke in a PWM forward converter, and it has an identical current-flux-swing requirement of $(V_O T/4) \cdot I_O$ for the worst case in which the regulation $\gamma = 0.5$. As such, the only "extra" component beyond those in a standard PWM forward converter is the nonlinear reactor, which serves the purpose of effecting zero-voltage switching and control. If the reactor is sized to be capable of reducing the output voltage from nominal to zero, each core has a flux-current stress of $(V_O T/8) \cdot I_O$. However, if it is unnecessary to be able to reduce the output voltage all the way to zero, the flux requirement is proportionally lower.

We are now prepared to compare the circuit with the similar circuit of [5-7], shown in Fig. 4. The saturating reactors in both circuits serve to delay the current reversal in the primary. However, in the circuit of Fig. 4, the reactors do not clamp the current waveform and force it to be square. Rather, the filter inductor L_O effectively clamps the diode and primary currents. Since the rectifier is inductively loaded, each diode will experience a switching loss at turn off, accompanied by a ringing transient.

A conventional PWM forward converter with a mag-amp post regulator suffers the same disadvantage of diode losses and high peak diode voltages. In addition, the primary-side devices experience switching losses.

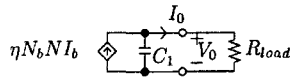


Fig. 5. Averaged dynamical model for effect of control current on output voltage.

III. AVERAGED CIRCUIT MODEL

Based on the above discussion, an approximate averaged circuit model can be developed for the purpose of modeling the low frequency dynamics of this circuit (Fig. 5). The output of the rectifier is replaced with its average value, which is assumed to be determined by the ideal nonlinear reactor clamp current, $N_b I_b$, multiplied by a scaling factor η ($0 < \eta < 1$), which accounts for the nonideal behavior discussed above, and multiplied by the turns ratio N of the main transformer.

IV. EXPERIMENTAL RESULTS

A low-frequency (25 kHz) converter was constructed to verify the waveforms predicted above. In addition, a 700 kHz circuit built with thick-film conductors on a ceramic substrate was constructed to demonstrate performance at higher frequencies with higher power density [12]. Because some measurement points on the 700 kHz circuit are difficult to access, and waveforms from the low-frequency prototype are more elucidative, the low-frequency prototype is discussed in more detail here.

For a practical implementation, there are several ways in which the bias current for the nonlinear reactor may be derived. One option is to supply the bias through a simple buck regulator, which can operate from the output voltage of the converter. If the number of turns on the bias winding is large, the buck circuit must handle only a small current, and its VA product rating can be a small fraction of the total circuit power rating. The average voltage on the bias winding is zero, and so the average power output of the converter need only be sufficient to supply the resistive losses in this winding. Thus, the efficiency and power density requirements for this converter are considerably relaxed, compared with the requirements for the main circuit. The choke in the buck circuit, however, must still support a substantial VA, as discussed in Section II.

Another option for supplying bias current to the reactor is shown in Fig. 6. Since a bias current proportional to output current is needed, one solution is to use the output current itself for bias. Since the reactor bias winding has an ac voltage across it, it is necessary to introduce an inductive output filter. This choke has the same VA rating as the choke needed for a buck converter supplying the bias winding. In this self-biased circuit, the control may still be effected by an isolated winding on the nonlinear reactor.

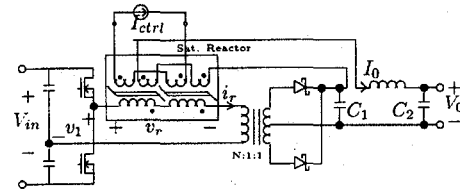


Fig. 6. Self-biasing arrangement.

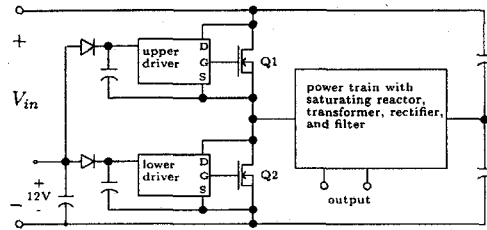


Fig. 7. Organization of gate drive.

However, the ampere-turn requirement for the control winding is small, theoretically zero. The choice of bias scheme depends on the requirements of a particular application. For our first prototypes we used the self-biased circuit, as shown in Fig. 6.

The simple, open-loop nature of the gate drive allows the use of a self-oscillating gate drive. In this scheme, the upper MOSFET is held on for a fixed duration $T/2$ while the lower MOSFET is held off. After this duration, the upper device is turned off. After the current in the nonlinear reactor commutates the capacitance on the inverter stage (v_1 in Fig. 6), the lower MOSFET gate drive circuit detects that the voltage has collapsed on the lower MOSFET, and immediately turns this device on for a complementary fixed duration $T/2$. As such, the conduction time for the MOSFET body diodes is minimized or eliminated. While the lower MOSFET is held on, the current in the nonlinear reactor switches polarity. The turn-off of the lower MOSFET occurs in an analogous manner to that of the upper MOSFET. Consequently, the primary side control is built around two independent self-timed gate drive circuits. It is not necessary to couple signals between the two drive circuits. A simple start-up circuit is needed and incorporated, however. Our implementation uses a commercially-available gate drive integrated circuit (IC) in combination with two CMOS NAND gates. Each gate drive section could easily be integrated into a single IC. Fig. 7 illustrates the overall organization of the gate drive scheme.

A. Low Frequency Prototype

The 25 kHz prototype was designed for a nominal input voltage of 40 V, a nominal maximum output voltage of 5 V, and maximum load current of 20 A. The transformer turns ratio was 4 : 1 : 1. The turns ratio on each core of the nonlinear reactor was 4 : 1 : 1. (The primary side winding had four times the number

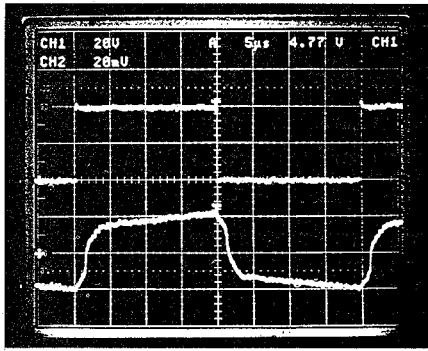


Fig. 8. 25 kHz prototype primary side waveforms. Top: V_{DS2} (20 V/div.). Bottom: I_{primary} (1 A/div.); 5 $\mu\text{s}/\text{div}$.

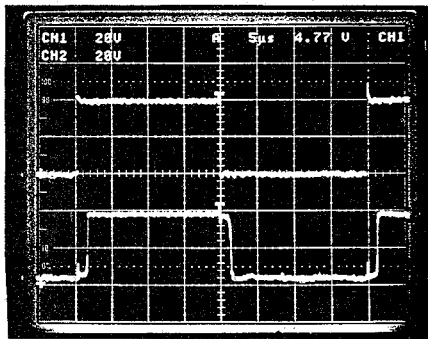


Fig. 9. 25 kHz prototype primary side waveforms. Top: V_{DS2} (20 V/div.). Bottom: $I_{\text{xformer-pri}}$ (20 V/div.); 5 $\mu\text{s}/\text{div}$.

of turns on the feedback winding, and four times the number of turns on the control winding.)

Fig. 8 shows the lower MOSFET drain-source voltage and the primary side reactor current of the 25 kHz circuit. As seen in this photograph, the current has a square characteristic and lags the switch voltage waveform. The reason for the non-zero slope of the top of the current waveform is the finite inductance of the output choke and finite magnetizing inductance of the nonlinear-reactor cores. The rounded corners of the current waveform are a result of the deviations from squareness of the $B-H$ characteristic of the saturating cores.

Fig. 9 shows the lower MOSFET drain-source voltage and the primary side transformer voltage. Note that the transformer voltage is approximately in phase with the primary current of Fig. 8. The phase shift evident in Fig. 9 is the mechanism by which the converter voltage conversion ratio is adjusted. The control of this phase shift is accomplished by adjusting the current I_{ctrl} (see Fig. 6) in the control winding of the nonlinear reactor, as discussed in Section II.

Fig. 10 shows the output voltage as a function of control current in the nonlinear reactor. The maximum operating range of the nonlinear reactor in this circuit was designed to allow only a limited range of control. In particular, for a nominal zero output voltage, the imposed flux swing on the nonlinear reactor is beyond

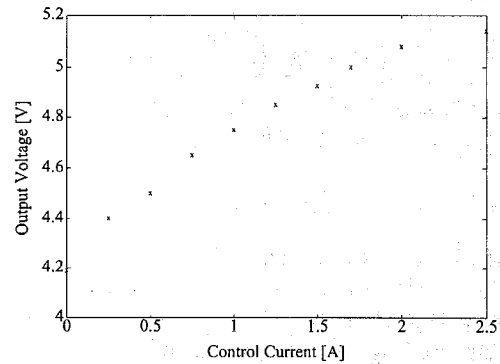


Fig. 10. Effect of control current on output voltage in 25 kHz prototype.

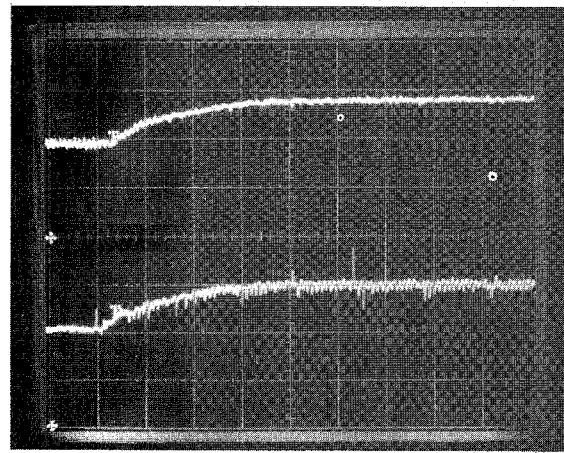


Fig. 11. 25 kHz prototype open-loop response to step in control current. Top: V_{out} (1 V/div.). Bottom: V_{C_1} (1 V/div.); 0.2 ms/div.

the maximum operating range indicated in Fig. 2. Hence, the circuit adjusts itself with zero control current to a minimal output voltage consistent with the characteristic of Fig. 2.

Fig. 11 shows the open-loop output response to a step change in control current, from zero to 1 A. Fig. 12 shows a simulation of an averaged circuit model. The averaged circuit model is based on that shown in Fig. 5, but is augmented to include the output choke and feedback from the bias winding as shown in Fig. 13. The bias winding itself, connected between the output choke and C_1 , is replaced by a short in the averaged model, recognizing that only high-frequency ac voltage appears across this winding. The simulation corresponds very closely with the experimental result. The value of η for the simulation was determined from measurements of circuit operation to be approximately 0.64. Both the simulation and the experiment had a 8.9 μH choke, 220 μF capacitors for both C_1 and C_2 , and a 0.52 Ω load resistor. The simulation differed from the model of Fig. 13 by having a dc offset equal to the dc offset observed in the experimental circuit added to the output voltage. This dc offset is due to the limited control range the nonlinear reactor was

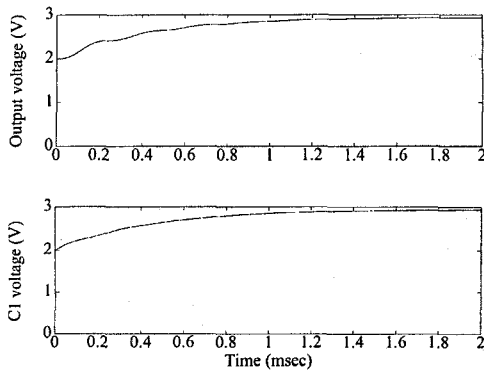


Fig. 12. Simulation of open-loop response to step in control current, based on averaged model in Fig. 13.

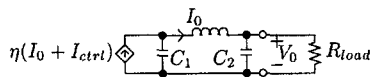


Fig. 13. Averaged model for self-biased circuit.

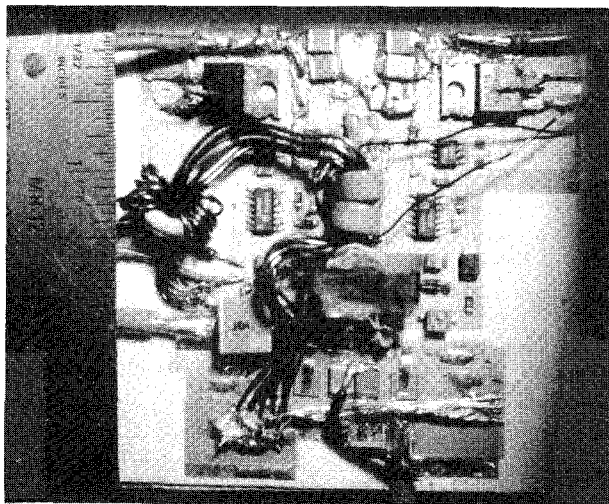


Fig. 14. 700 kHz prototype.

designed to effect, as discussed above. Note that the closed-loop system would have a faster response. Open-loop responses are shown here for the purpose of verifying the averaged model.

B. 700 kHz Prototype

A 700 kHz prototype, shown in Fig. 14, was fabricated on a 0.025 in (0.64 mm) thick alumina substrate, with silver thick-film conductors [12]. Although a larger substrate was used for convenience, the active area used was approximately $3 \times 2 \text{ in}^2$ ($8 \times 5 \text{ cm}^2$).

The transformer was constructed on a small ferrite “EI” core, 0.41 in (10.5 mm) high. The saturating reactors were built with a pair of amorphous metal alloy cores (Toshiba MB-8). The transformer and reactor were wound with Litz wire, with multiple paralleled interleaved windings to reduce leakage inductance and proximity effect.

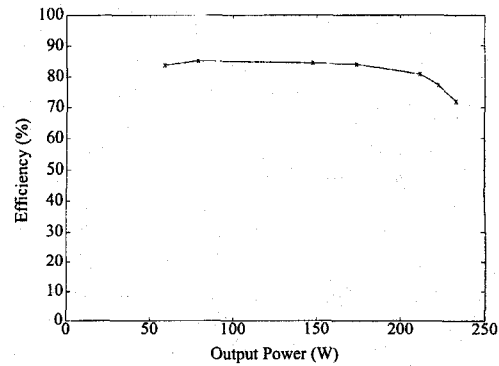


Fig. 15. Measured efficiency of 700 kHz prototype.

The measured efficiency of the 700 kHz prototype with 40 V input and output near 6.5 V is shown in Fig. 15. Although our objective was not to maximize power density, we note that this corresponds to approximately 70 W/in^3 (1100 W/cm^3), without the heat sink volume, or 45 W/in^3 (740 W/cm^3) including the heat sink volume. We expect to achieve higher power and efficiency once several problems with the initial prototype are solved. First, the nonlinear reactor in the current prototype overheats, due to excessive losses and a poor thermal path. We are investigating improved methods of fabricating this component [13–15]. Our second major limitation preventing improved performance at high power is a higher than expected resistivity of the silver conductor on the board. This was improved somewhat by soldering copper wire to the exposed conductors. However, some of the lower layer conductors were not accessible, and their losses could not be reduced.

Despite these problems, the prototype did verify the viability of this topology for operation at high frequency. The waveforms shown in Fig. 16 show that zero voltage switching was achieved on the MOSFETs. Some ringing is evident on the diode voltage, due to imperfect coupling between the two transformer secondaries, but it is small, and represents only about 0.1 W of loss. Control by means of the nonlinear reactor functioned as expected, although overheating quickly lowered its flux capacity and decreased the control range. Although measurements of core loss were not practical in the circuit, and the manufacturer does not provide core loss data for frequencies this high, it appears that a different core material is necessary to make the circuit practical at frequencies above about 500 kHz.

V. VARIATIONS AND EXTENSIONS

The features of this circuit lend it to applications in many different configurations. For multioutput supplies, multiple power trains may be connected to the same half-bridge. Each output is then controlled by a separate control windifg, but they share the same inverter bridge and gate-drive circuits. The windings

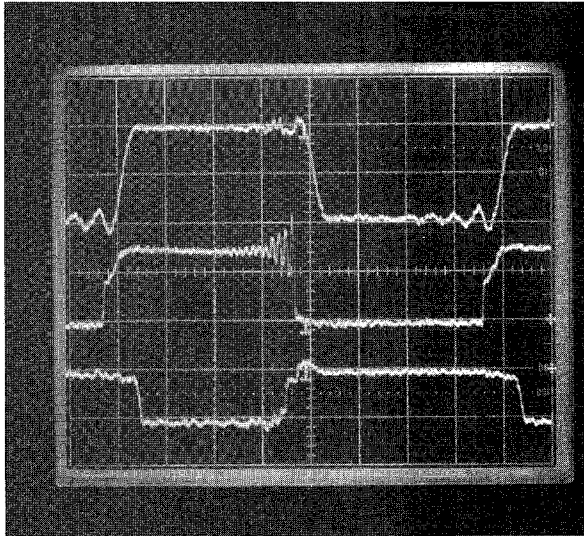


Fig. 16. Waveforms of 700 kHz prototype with 40 V input, 6.2 V, 27 A output. Top: V_{GS2} (10 V/div.). Middle: rectifier voltage, (10 V/div.). Bottom: V_{DS2} (20 V/div.); 200 ns/div.

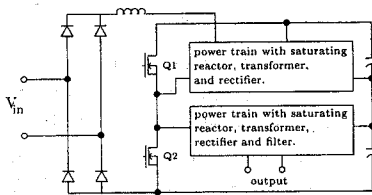


Fig. 17. High power factor circuit.

of the saturating reactor may be reconfigured in such a way as to allow it to be connected on the secondary side of the transformer, allowing multiple outputs to share the same transformer. Placing the reactor on the secondary side also allows the use of a push-pull primary configuration. Multiple outputs can also be used to construct a high power factor supply, using the approach of [16, 17], as shown in Fig. 17. In all of these circuits, the lack of a need for signals passing through isolation barriers is an important advantage. The need for gate-drive signal isolation is avoided by the use of the open-loop gate drive. The control winding is inherently isolated, and may be connected to a regulator circuit referenced to the isolated circuit it is controlling, or to the primary in the case of the high-power-factor circuit.

VI. CONCLUSION

The dc-dc converter presented features constant-frequency operation, zero-voltage-switching, and square current and voltage waveforms. A nonlinear magnetic element produces the advantageous square waveforms, and provides isolated terminals from which the output voltage may be controlled. All of the semiconductor devices exhibit very low switching losses. The primary active switches

exhibit zero-voltage switching. The output rectifier circuit has switching losses only due to the leakage inductance between the two secondary windings on the output transformer, which may be kept very small. The active switches (MOSFET's) are operated at a fixed frequency with 50% duty cycle, which allows the use of a simple open-loop gate drive scheme. Experimental half-bridge implementations demonstrated operation as expected. The circuit is applicable to high-power factor converters and multioutput supplies, as well as dc-dc converters.

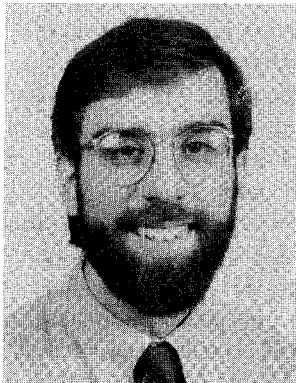
ACKNOWLEDGMENT

The authors thank Alain DeLeon for constructing and testing the low frequency prototype.

REFERENCES

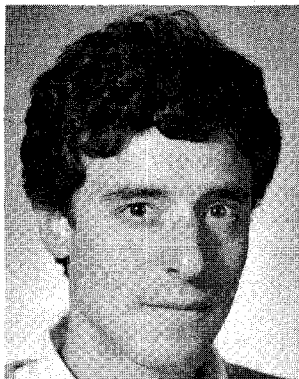
- [1] Patterson, O., and Divan, D. (1991) Pseudo-resonant full bridge dc/dc converter. *IEEE Transactions on Power Electronics*, 6 (Oct. 1991), 671-678.
- [2] Mweene, L., Wright, C., and Schlecht, M. (1991) A 1 kW 500 kHz front-end converter for a distributed power supply system. *IEEE Transactions on Power Electronics*, 6 (July 1991), 398-407.
- [3] Fisher, R., Ngo, K., and Kuo, M. (1988) A 500 kHz, 250 W dc-dc converter with multiple outputs controlled by phase-shifted pwm and magnetic amplifiers. In *High Frequency Power Conversion Conference Proceedings*, May 1988, 100-110.
- [4] Redl, R., Sokal, N., and Balogh, L. (1991) A novel soft-switching full-bridge dc/dc converter: Analysis, design considerations, and experimental results at 1.5 kw, 100 kHz. *IEEE Transactions on Power Electronics*, 6 (July 1991), 408-418.
- [5] Hamada, S., and Nakaoka, M. (1991) Analysis and design of a saturable reactor assisted soft-switching full-bridge dc-dc converter. In *Proceedings of 22nd Annual Power Electronics Specialists Conference*, June 1991, 155-162.
- [6] Hamada, S., Maruyama, Y., and Nakaoka, M. (1992) Saturable reactor assisted soft-switching technique in PWM dc-dc converters. In *Proceedings of 23rd Annual Power Electronics Specialists Conference*, June 1992, 93-100.
- [7] Farrington, R., Jovanovic, M., and Lee, F. (1991) A new family of isolated zero-voltage switched converters. In *Proceedings of 22nd Annual Power Electronics Specialists Conference*, June 1991, 209-215.
- [8] Jamerson, C., and Chen, D. (1993) Magamp postregulators for symmetrical topologies with emphasis on half-bridge configuration. *IEEE Transactions on Power Electronics*, 8 (Jan. 1993), 26-29.
- [9] Vollin, J., Tan, F., and Cuk, S. (1993) Magnetic regulator modeling. In *Proceedings Applied Power Electronics Conference (APEC)*, Mar. 1993, 604-611.

- [10] Erickson, R., Hernandez, A., Witulski, A., and Xu, R. (1990)
A nonlinear resonant switch.
In *Proceedings of 21st Annual Power Electronics Specialists Conference*, June 1990, 43–50.
- [11] Gu, W., and Harada, K. (1992)
A novel, self-excited, PWM forward converter with ZVS resonant transitions using two minor-loop operated saturable cores.
In *Proceedings of 23rd Annual Power Electronics Specialists Conference*, June 1992, 85–92.
- [12] Sullivan, C. R., and Sanders, S. R. (1993)
A soft-switched constant-frequency square-wave half-bridge dc-dc converter.
In *Proceedings of 24th Annual Power Electronics Specialists Conference*, June 1993, 158–166.
- [13] Sullivan, C. R., and Sanders, S. R. (1993)
Microfabrication of transformers and inductors for high frequency power conversion.
In *Proceedings of 24th Annual Power Electronics Specialists Conference*, June 1993, 33–40.
- [14] Sullivan, C. R., and Sanders, S. R. (1995)
Microfabrication process for high-frequency power-conversion transformers.
In *Proceedings of 26th Annual Power Electronics Specialists Conference*, June 1995, 658–664.
- [15] Sullivan, C. R., and Sanders, S. R. (1996)
Microfabrication of transformers and inductors for high frequency power conversion.
IEEE Transactions on Power Electronics, **11** (Mar. 1996), 228–238.
- [16] Kheraluwala, M. H., Steigerwald, R. L., and Gurumoorthy, R. (1991)
A fast-response high power factor converter with a single power stage.
In *Proceedings of 22nd Annual Power Electronics Specialists Conference*, June 1991, 769–779.
- [17] Steigerwald, R. L., and Kornumpf, W. P. (1987)
Power circuit with high input power factor and a regulated output.
U.S. Patent 4,642,745, Mar. 1987.



Charles R. Sullivan (S'93—M'96) was born in Princeton, NJ, in 1964. He received a B.S. in electrical engineering from Princeton University, Princeton, NJ, in 1987, and a Ph.D. in electrical engineering and computer sciences from the University of California, Berkeley, in 1996. Between 1987 and 1990 he worked at Lutron Electronics, Coopersburg, PA, developing high frequency dimming ballasts for compact fluorescent lamps. He is presently Assistant Professor at the Thayer School of Engineering, at Dartmouth College, in Hanover, NH.

Dr. Sullivan has published technical papers on topics including thin-film magnetics for high frequency power conversion, dc-dc converter topologies, energy and environmental issues, and modeling, analysis, and control of electric machines.



Seth R. Sanders (M'87) received S.B. degrees in electrical engineering and physics in 1981, S.M. and Ph.D. degrees in electrical engineering in 1985 and 1989, respectively, all from M.I.T., Cambridge, MA.

He worked as a design engineer at the Honeywell Test Instruments Division in Denver, CO, from 1981–1983. He is presently Associate Professor in the Department of Electrical Engineering and Computer Sciences at the University of California, Berkeley. During the 1992–1993 academic year, he was on industrial leave with National Semiconductor in Santa Clara, CA. His research interests are in power electronics, variable speed drive systems, simulation, and in nonlinear circuit and system theory as related to the power electronics field.

Dr. Sanders is a recipient of the NSF Young Investigator Award in 1993, and presently serves as Chair of the IEEE Technical Committee on Computers in Power Electronics.